

Ti₄Ir₂O a time-reversal-invariant fully gapped unconventional superconductor

Debarchan Das,¹ KeYuan Ma,² Jan Jaroszynski,³ Vahid Sazgari,¹
Tomasz Klimczuk,^{4,5} Fabian O. von Rohr,⁶ and Zurab Guguchia¹

¹Laboratory for Muon Spin Spectroscopy, Paul Scherrer Institute, CH-5232, Villigen PSI, Switzerland

²Max Planck Institute for Chemical Physics of Solids, 01187 Dresden, Germany

³National High Magnetic Field Laboratory, Florida State University, Tallahassee, Florida 32310, USA

⁴Faculty of Applied Physics and Mathematics, Gdansk University of Technology,
ul. Narutowicza 11/12, Gdańsk 80-233, Poland

⁵Advanced Materials Centre, Gdansk University of Technology,
ul. Narutowicza 11/12, Gdańsk 80-233, Poland

⁶Department of Quantum Matter Physics, University of Geneva, CH-1211 Geneva, Switzerland

Here we report muon spin rotation (μ SR) experiments on the temperature and field dependence of the effective magnetic penetration depth $\lambda(T)$ in the η -carbide-type suboxide Ti₄Ir₂O, a superconductor with an considerably high upper critical field. Temperature dependence of $\lambda(T)$, obtained from transverse-field (TF)- μ SR measurements, is in perfect agreement with an isotropic fully gapped superconducting state. Furthermore, our ZF μ SR results confirm that the time-reversal symmetry is preserved in the superconducting state. We find, however, a remarkably small ratio of $T_c/\lambda_0^{-2} \sim 1.22$. This value is close to most unconventional superconductors, showing that a very small superfluid density is present in the superconducting state of Ti₄Ir₂O. The presented results will pave the way for further theoretical and experimental investigations to obtain a microscopic understanding of the origin of such a high upper critical field in an isotropic single gap superconducting system.

The quest for superconducting materials for ground-breaking applications continues to drive the condensed matter research community, leading to the discovery of an array of novel superconductors and improved superconducting properties. [1]. A lot of research effort has been put forward to advance novel superconducting materials with improved properties such as high transition temperature (T_c), high value of critical current, and of upper critical field (H_{c2}). Furthermore, high upper critical fields H_{c2} are of interest from a fundamental point of view, as these are commonly associated with unconventional, possibly even topological, superconductivity.[2–4] High-upper critical fields are also associated with unusual field-induced superconducting states, such as e.g., the Fulde-Ferrell-Larkin-Ovchinnikov (FFLO) state, which is a distinct superconducting phase observed in spin-singlet superconductors.[5–7]

One recent approach to control the properties of superconductors has been the chemically precise filling of void position in the crystal structures using electron-donor atoms to chemically tune the electronic properties of these materials.[8, 9] Along this line, η -carbide-type oxides turn out to be a promising material platform since it results from filling void positions in the Ti₂Ni-type structure, with small non-metallic atoms such as oxygen, nitrogen, or carbon occupying the interstitial positions[15].

η -Carbide family of compounds, encompasses a variety of materials which are important for the investigation of emergent quantum properties [10–14]. Most importantly, some members of this family exhibit superconductivity [10, 14, 16]. One notable example is Ti₄Ir₂O which manifests superconducting properties with a critical temperature of $T_c \simeq 5.3$ K along with a considerably high upper critical field of $\mu_0 H_{c2} \sim 16$ T as revealed from bulk measurements[10]. Interestingly, the H_{c2} exceeds

the weak-coupling Pauli limit ($\mu_0 H_{Pauli} \approx 9.8$ T) which corresponds to the paramagnetic pair breaking effect governing the maximal H_{c2} in conventional superconductors [17]. Recent DFT calculations revealed the presence of multiple bands crossing at the Fermi energy E_F signaling plausible multi-gap superconductivity in Ti₄Ir₂O. Moreover, there is a pronounced peak of density of states close to E_F , arising from the weakly dispersing energy bands[16]. This aspect resembles a key aspect of the recently widely discussed flat-band kagome superconductors [18–21]. Most recently, it was found that Ti₄Ir₂O maybe the first fully isotropic FFLO superconductor, in contrary to the previous candidates, which all display highly anisotropic layered structures.[22]

To gain insight into the superconducting properties of Ti₄Ir₂O, we conducted muon spin rotation/relaxation (μ SR) experiments, a technique highly sensitive to superconducting gap structures in materials [23–25]. Using transverse field (TF) μ SR in type-II superconductors, we can assess the temperature dependence of the magnetic penetration depth λ , crucial for understanding the superconducting gap structure. Additionally, zero-field (ZF) μ SR is effective for detecting very small internal magnetic fields, ideal for exploring spontaneous magnetic fields related to broken time-reversal symmetry in exotic superconductors [26–32].

In this letter, we report on the low density of copper pairs (dilute superfluid) and unusually high upper critical field larger than the Pauli limit in η -carbide-type suboxide Ti₄Ir₂O. We, furthermore, demonstrate the isotropic fully gap pairing and the preserved time-reversal symmetry in the SC state of this system. These results identify Ti₄Ir₂O as time-reversal-invariant fully gapped unconventional superconductor.

Polycrystalline Ti₄Ir₂O samples were synthesized from

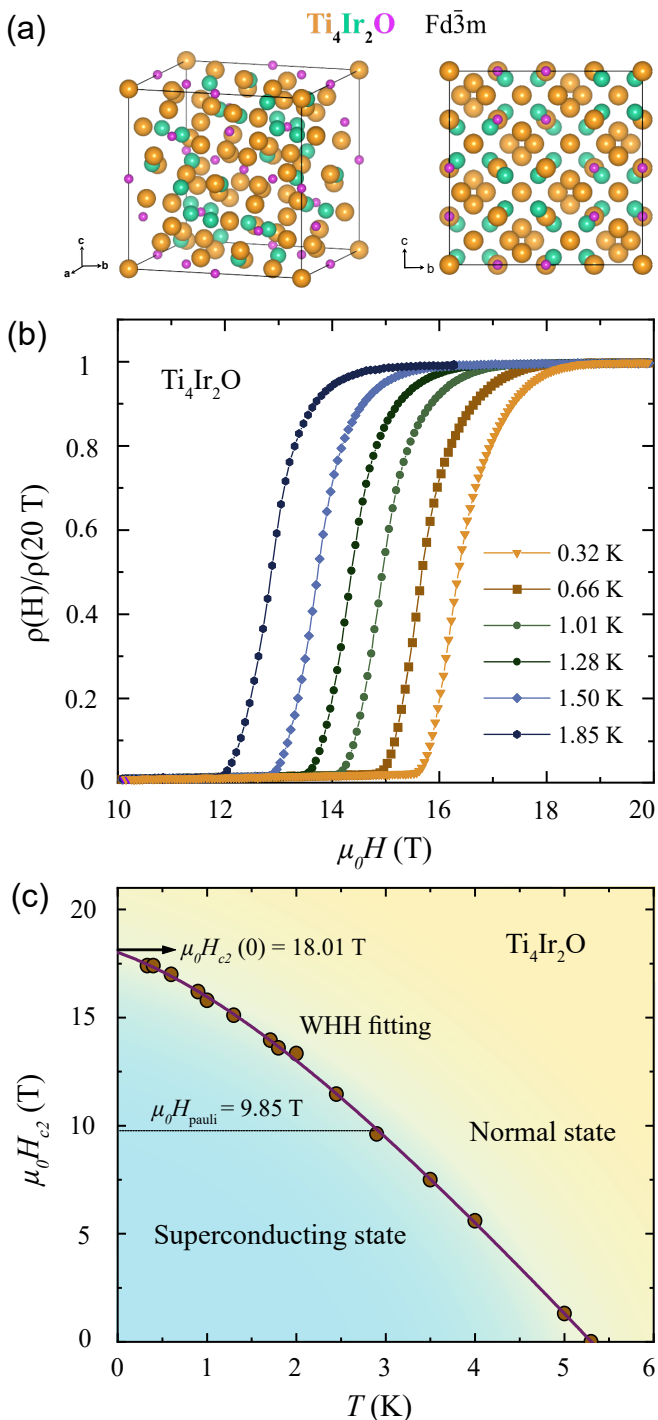


FIG. 1. (a) Schematic representation of two orientations for the crystal structure of $\text{Ti}_4\text{Ir}_2\text{O}$, (b) high magnetic field (10 - 20 T) transport measurement of $\text{Ti}_4\text{Ir}_2\text{O}$ at low temperatures down to 300 mK (c) $\mu_0 H_{c2}(T)$ phase diagram of $\text{Ti}_4\text{Ir}_2\text{O}$ determined from electrical transport measurements under external fields. The solid purple line represents the fitting of the experimental data with Werthamer-Helfand-Hohenberg (WHH) expression.

high-purity titanium (purity: 99.9%, Alfa Aesar), irid-

ium (purity: 99.99%, Strem Chemicals), and titanium dioxide powders (purity: 99.9%, Sigma-Aldrich) via arc-melting and solid-state reaction. Initially, the reactants were mixed in stoichiometric ratios, formed into a pellet, and melted in an arc furnace under a purified argon atmosphere to ensure homogeneity. The resulting melt was then ground into fine powders, re-pelletized, and annealed in a sealed quartz tube at 1000 °C for 7 days under a partial argon atmosphere. The reaction was completed by cooling the quartz tube to room temperature through water quenching.

For magneto-transport measurements, a bar shaped sample was used with four 50 μm dia platinum wire leads spark-welded to the sample surface. The transport measurements were performed in the 35 T resistive magnet at the National High Magnetic Field Laboratory. The magnet was swept from 11.5 T to 20 T owing to the static 11.5 T background field generated by the outer superconducting coil of the magnet combination. The temperature under 2 Kelvin was ascertained using the vapor pressure of Helium-3, which remains unaffected by magnetic fields. This method contrasts with the use of Cernox and Ruthenium Oxide thermometers, which exhibit significant magnetoresistance. Transport measurements in lower fields were performed using a Physical Properties Measurements System (PPMS) from Quantum Design, equipped with a 9T superconducting magnet.

Transverse-field (TF) and zero-field (ZF) μSR experiments were carried out at πE1 beamline on DOLLY spectrometer at the Paul Scherrer Institute (Villigen, Switzerland). The field dependent TF- μSR experiments at 1.6 K were performed at $\pi\text{M3.2}$ beamline using GPS spectrometer. For μSR experiments, we used powdered sample which was pressed into a 7 mm pellet and then mounted on a Cu holder using GE varnish. This holder assembly was then mounted in the respective spectrometer cryostat. Both spectrometers are equipped with a standard veto setup [33] providing a low-background μSR signal. All the TF experiments were performed after field-cooled-cooling the sample. The μSR time spectra were analyzed using the MUSRFIT software package [34].

$\text{Ti}_4\text{Ir}_2\text{O}$ crystallizes in the η -carbide type structure in the cubic space group $Fd\bar{3}m$, with a unit cell parameter of $a = 11.62931(2)$ Å at room temperature [10]. In Figure 1(a), we show a schematic view of the $\text{Ti}_4\text{Ir}_2\text{O}$ crystal structure along two orientations. The number of atoms in the unit cell is 112, of which 96 are metal atoms and 16 are oxygen. In the structure, titanium atoms occupy the $16c$ and the $48f$ Wyckoff positions, iridium atoms occupy the $32e$ Wyckoff positions, and oxygen atoms occupy the $16d$ Wyckoff positions, resulting in a formula of $\text{Ti}_{64}\text{Ir}_{32}\text{O}_{16}$ for one unit cell [10]. The prepared polycrystalline $\text{Ti}_4\text{Ir}_2\text{O}$ samples were found to be single phase by means of powder X-ray diffraction measurement.

In Figure 1(b), we present high magnetic field (20 T) transport measurement of $\text{Ti}_4\text{Ir}_2\text{O}$ down to 320 mK. The data was plot as the normalized resistivity $\rho(H)/\rho(20\text{ T})$

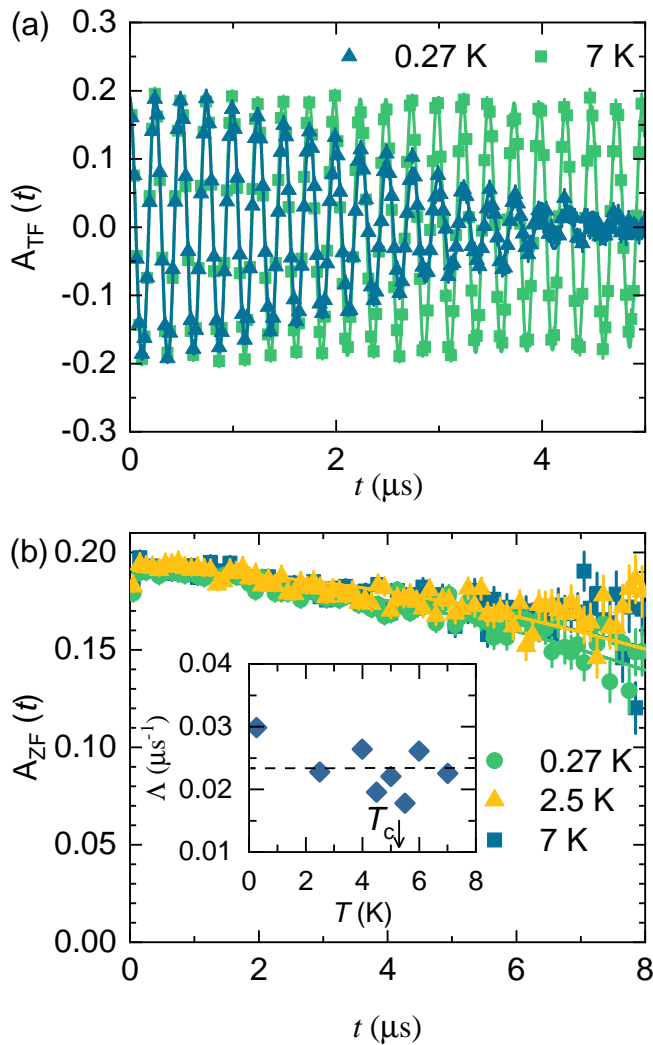


FIG. 2. (a) TF μ SR time domain spectra obtained above and below T_c for $\text{Ti}_4\text{Ir}_2\text{O}$ in an applied field of 30 mT (after field cooling the sample from above T_c). (b) ZF μ SR asymmetry spectra recorded at 0.27 and 7 K for $\text{Ti}_4\text{Ir}_2\text{O}$. Inset: temperature dependence of the electronic relaxation rate measured in zero magnetic field.

versus magnetic field $\mu_0 H(\text{T})$ at different constant below the critical temperature T_{rmc} . We can clearly observe the transition to the normal state from the superconducting state at high magnetic fields under all measured temperatures. Here, we determined the superconducting transition critical field $\mu_0 H(\text{T})$ at different temperatures as a midpoint of the transition. These high magnetic field transport measurement data together with those measured under lower fields were used to obtain the upper critical field $\mu_0 H_{c2}(0)$ as shown in Figure 1(c).

The upper critical field $\mu_0 H_{c2}(0)$ of $\text{Ti}_4\text{Ir}_2\text{O}$ was estimated using the Werthamer-Helfand-Hohenberg (WHH) approximation in the clean limit[10]:

$$\mu_0 H_{c2}(T) = \frac{\mu_0 H_{c2}(0)}{0.73} h_{fit}^*(T/T_c). \quad (1)$$

$$h_{fit}^*(t) = (1-t) - C_1(1-t)^2 - C_2(1-t)^4. \quad (2)$$

where $t = T/T_c$ and T_c (5.30 K) is the transition temperature at zero magnetic field. In Figure 1(c), we show the $\mu_0 H_{c2}(0)$ fitting of $\text{Ti}_4\text{Ir}_2\text{O}$ using the Werthamer-Helfand-Hohenberg (WHH) approximation in the clean limit. We found the fitting line fairly well describes all the obtained experimental points, where $\mu_0 H_{c2}(0)$ was determined to be 18.01 T. This value is exceeding by far than the Pauli paramagnetic limit $\mu_0 H_{\text{Pauli}}$ of 9.85 T, which is derived from $\mu_0 H_{\text{Pauli}} \approx 1.86[\text{T/K}] \cdot T_c$ for a weak-coupling BCS superconductor. Here, this unusual high upper critical field indicates an unconventional superconductivity behavior in $\text{Ti}_4\text{Ir}_2\text{O}$.

Figure 2a shows TF- μ SR spectra for $\text{Ti}_4\text{Ir}_2\text{O}$ measured in an applied magnetic field of 30 mT at temperatures above (7 K) and below (0.27 K) the critical temperature T_c . A small relaxation, observed in TF- μ SR spectra above T_c , can be attributed to the presence of random local fields associated with the nuclear magnetic moments. In the superconducting state, the formation of FLL creates an inhomogeneous distribution of magnetic field which leads to the increase of the relaxation rate of the μ SR signal below T_c .

Magnetism, if present in the samples, may also enhance the muon depolarization rate and influence the interpretation of the TF- μ SR results. Therefore, we have carried out ZF- μ SR experiments above and below T_c to search for magnetism (static or fluctuating) in $\text{Ti}_4\text{Ir}_2\text{O}$. As seen from Fig. 2b, we do not observe any noticeable difference in ZF- μ SR asymmetry spectra recorded at temperatures above and below T_c . The ZF- μ SR asymmetry spectra can be well described by an exponential decay function, $A_{ZF}(t) = A_0 G_{KT} \exp(-\Lambda t)$ where A_0 is the initial asymmetry and Λ is the depolarization rate. The inset of Fig. 2b shows the temperature evolution of Λ , which shows no noticeable enhancement across T_c . The maximum possible spontaneous flux density due to superconductivity can be estimated using $(\Lambda|_{0.27\text{ K}} - \Lambda|_{7\text{ K}})/(2\pi\gamma_\mu) = 1.49 \mu\text{T}$ which is several times smaller than that seen for well known TRS breaking superconductors [27, 28]. This demonstrates the absence of any spontaneous field in either the normal or the superconducting state of $\text{Ti}_4\text{Ir}_2\text{O}$. Therefore, this sample is non-magnetic and also the time-reversal symmetry is preserved in the superconducting state of this compound.

The absence of magnetism in $\text{Ti}_4\text{Ir}_2\text{O}$ implies that the increase of the TF relaxation rate below T_c is attributed entirely to the flux-line lattice (FLL). Assuming a Gaussian field distribution, we analyzed the observed TF- μ SR asymmetry spectra using the following functional form

$$A_{\text{TF}}(t) = A_0 \exp(\sigma^2 t^2 / 2) \cos(\gamma_\mu B_{\text{int}} t + \varphi) \quad (3)$$

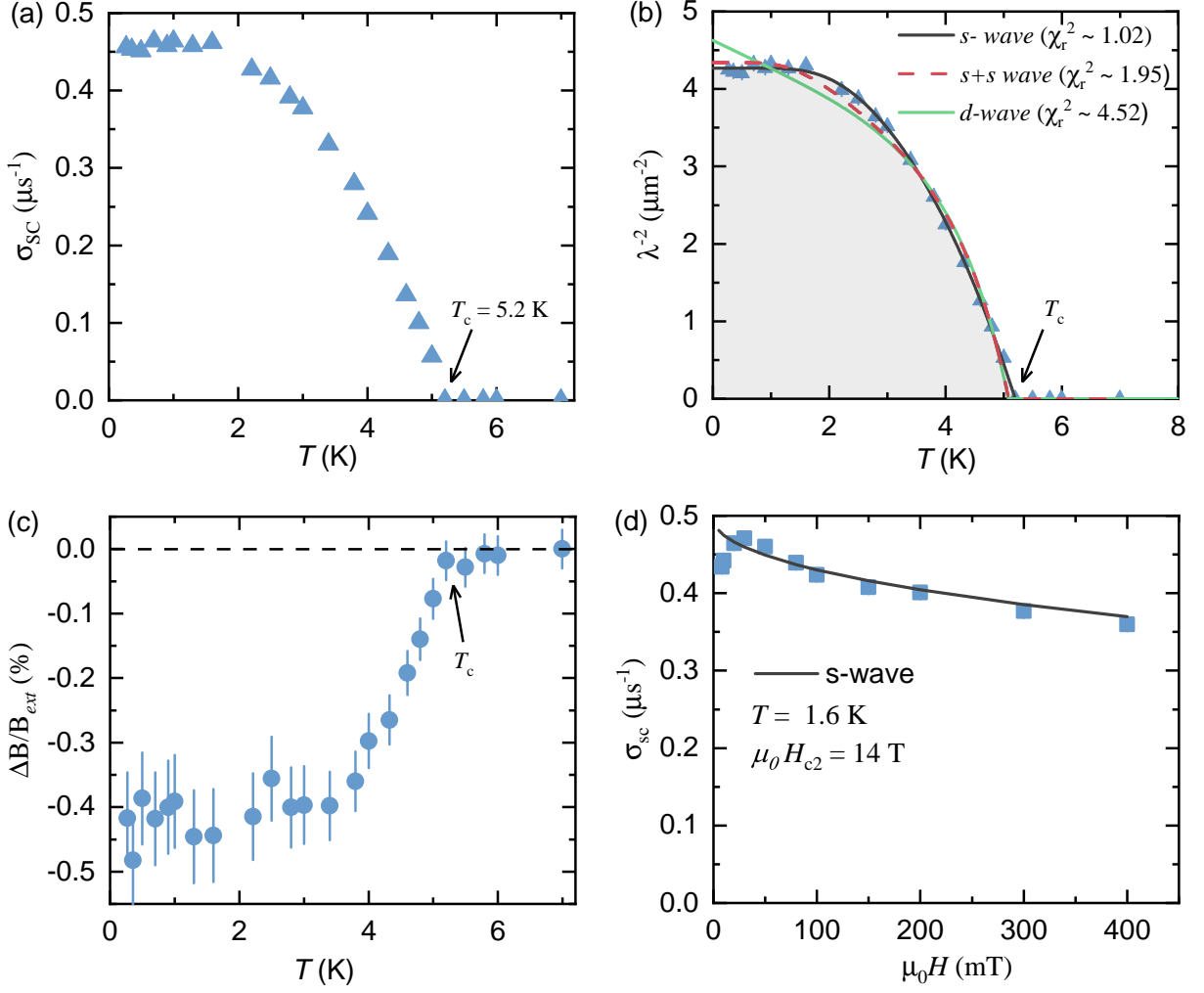


FIG. 3. (a) Temperature evolution of the superconducting muon spin depolarization rate σ_{sc} of $\text{Ti}_4\text{Ir}_2\text{O}$ measured in an applied magnetic field of 30 mT. (b) Temperature evolution of $\lambda^{-2}(T)$ measured in an applied field $\mu_0 H = 30$ mT. The solid and dashed lines represent fitting with different theoretical models as discussed in the text. For $s+s$ -wave fitting, we fixed the gap values obtained from heat capacity data[16]. (c) Temperature dependence of the relative change of the internal field normalized to the external applied field, $\Delta B/B_{\text{ext}}$ ($= \frac{B_{\text{int}} - B_{\text{ext}}}{B_{\text{ext}}}$). (d) The field dependence of TF-relaxation rate $\sigma_{\text{sc}}(B)$ measured at 1.6 K

where A_0 refers to the initial asymmetry, $\gamma_\mu \simeq 851.615$ MHz/T is the muon gyromagnetic ratio, and φ is the initial phase of the muon-spin ensemble, B_{int} corresponds to the internal magnetic field at the muon site, respectively and σ is the total relaxation rate. σ is correlated to the superconducting relaxation rate, σ_{sc} , following the relation $\sigma = \sqrt{\sigma_{\text{nm}}^2 + \sigma_{\text{sc}}^2}$ where σ_{nm} is the nuclear contributions that is assumed to be temperature independent. To estimate σ_{sc} , we considered the value of σ_{nm} obtained above T_c where only nuclear magnetic moments contribute to the muon depolarization rate σ . The solid lines in Fig. 1b depicts the fits to the observed spectra with Eq. 3.

In Figure 3a, we have presented σ_{sc} as a function of temperature for $\text{Ti}_4\text{Ir}_2\text{O}$ measured at an applied field of 30 mT. Below T_c , the relaxation rate σ_{sc} increases from zero due to inhomogeneous field distribution caused by

the formation of FLL, and saturates at low temperatures. In the following section, we show that the observed temperature dependence of σ_{sc} , which reflects the topology of the superconducting gap, is consistent with the presence of the single gap on the Fermi surface of $\text{Ti}_4\text{Ir}_2\text{O}$. Figure 3c shows the temperature dependence of the relative change of the internal field normalized to the external applied field, $\Delta B/B_{\text{ext}}$ ($= \frac{B_{\text{int}} - B_{\text{ext}}}{B_{\text{ext}}}$). As seen from the figure, internal field values in the superconducting state (*i.e.* $T < T_c$) are lower than the applied field because of the diamagnetic shift, expected for type-II superconductors.

For a perfect triangular vortex lattice, $\sigma_{\text{sc}}(T)$ is directly related to the London magnetic penetration depth

$\lambda(T)$ by [35, 36]:

$$\frac{\sigma_{sc}^2(T)}{\gamma_\mu^2} = 0.00371 \frac{\Phi_0^2}{\lambda^4(T)}. \quad (4)$$

where, $\Phi_0 = 2.068 \times 10^{-15}$ Wb is the magnetic flux quantum. It is important to note that Eq. 4 is valid when the separation between the vortices is smaller than λ [35]. We have analyzed the temperature dependence of the magnetic penetration depth, $\lambda^{-2}(T)$ to unveil the superconducting gap structure of $\text{Ti}_4\text{Ir}_2\text{O}$.

Within the London approximation ($\lambda \gg \xi$), $\lambda(T)$ can be described by the following expression, [17, 34, 37]

$$\frac{\lambda^{-2}(T, \Delta_{0,i})}{\lambda^{-2}(0, \Delta_{0,i})} = 1 + \frac{1}{\pi} \int_0^{2\pi} \int_{\Delta(T, \varphi)}^\infty \left(\frac{\partial f}{\partial E} \right) \frac{E dE}{\sqrt{E^2 - \Delta_i(T, \varphi)^2}}, \quad (5)$$

where $f = [1 + \exp(E/k_B T)]^{-1}$ is the Fermi function, φ is the azimuthal angle along the Fermi surface and $\Delta_{0,i}(T) = \Delta_{0,i} \Gamma(T/T_c) g(\varphi)$. $\Delta_{0,i}$ is the maximum gap value at $T = 0$ K. The temperature dependence of the gap is described by the expression $\Gamma(T/T_c) = \tanh \left\{ 1.82 [1.018 (T_c/T - 1)]^{0.51} \right\}$ [38]. For s -wave gap and a nodal d -wave, the angular dependence $g(\varphi)$ corresponds to 1 and $|\cos(2\varphi)|$ respectively. We have considered three models in our analysis: (i) an isotropic s -wave gap, (ii) a combination of two s -wave gaps of different size, and (iii) a nodal d wave model.

As seen from the Figure 3b, the experimentally obtained $\lambda^{-2}(T)$ dependence can be best described using a single s -wave model yielding a gap value of $\Delta_0 = 0.92(8)$ meV and $T_c = 5.19(3)$ K. Previously from heat capacity analysis, Ruan *et al.*[16] predicted the presence of two superconducting gaps ($\Delta_{0,1} = 1.37$ meV and $\Delta_{0,2} = 0.57$ meV). Therefore, to test this possible multi-gap scenario, we used these gap values and kept them fixed in our analysis.

For the two-gap scenario, we have used the weighted sum of two gaps:

$$\frac{\lambda^{-2}(T)}{\lambda^{-2}(0)} = x \frac{\lambda^{-2}(T, \Delta_{0,1})}{\lambda^{-2}(0, \Delta_{0,1})} + (1-x) \frac{\lambda^{-2}(T, \Delta_{0,2})}{\lambda^{-2}(0, \Delta_{0,2})}. \quad (6)$$

Here x is the weight associated with the larger gap and $\Delta_{0,i}$ ($i = 1, 2$ are the gap indices) are the gaps.

A close look at the goodness of fitting suggests that the single s -wave model gives the lowest value of χ_r^2 indicating the best fit to the observed data. We note that while fitting the experimental data keeping two gaps as free parameters, the weight of the higher gap (x) was reaching a value close to 0, implying the single gap scenario is more appropriate. Also d -wave gap symmetry was also tested, but were found to be inconsistent with the data (for example, see the green solid line in Fig 3b). Thus, from the μSR experiments, we confirm the presence of a single fully-gapped superconducting state in $\text{Ti}_4\text{Ir}_2\text{O}$.

We also investigated the field dependence of TF-relaxation rate $\sigma_{sc}(B)$ measured at 1.6 K (see Fig 3d).

For these measurements, each point was obtained by field-cooling the sample from 10 K (above T_c) to 1.6 K. σ_{sc} first increases to a maximum with increasing magnetic field followed by a continuous decrease up to the highest field (400 mT) studied as expected for a single gap superconductor with an ideal triangular vortex lattice. Interestingly, the observed $\sigma_{sc}(B)$ curve at fields above the maximum, can be well modelled using the Brandt formula (for a single s -wave gap superconductor) [36] with an upper critical field $\mu_0 H_{c2}(0.27 \text{ K}) = 14 \text{ T}$ at 1.6 K.

While the temperature- and field-dependence of the London penetration depth λ_{eff}^{-2} and henceforth of the superfluid density can be well understood as a fully gapped s -wave superconductor, the T_c/λ_{eff}^{-2} ratio for $\text{Ti}_4\text{Ir}_2\text{O}$ is comparable to those of high-temperature unconventional superconductors. In the context of the Bose-Einstein Condensation (BEC) to BCS crossover [39], systems with a small ratio of T_c/λ_{eff}^{-2} (approximately 0.00025-0.015) are categorized on the BCS-like side, indicative of conventional superconductivity. In contrast, a large ratio in the range of 1-20, along with a linear relationship between T_c and λ_{eff}^{-2} , is typically observed on the BEC-like side, signifying unconventional superconductivity. This framework has been historically utilized to differentiate between BCS-like (conventional) and BEC-like (unconventional) superconductors. The results obtained for $\text{Ti}_4\text{Ir}_2\text{O}$ show a ratio of $T_c/\lambda_{eff}^{-2} \simeq 1.22$, closely aligning with the ratio of approximately 1 seen in electron-doped cuprates. This finding, alongside previously reported high upper critical fields and thermodynamic evidence of an FFLO state, provides strong support for an unconventional pairing mechanism in $\text{Ti}_4\text{Ir}_2\text{O}$.

In conclusion, we provide the first microscopic investigation of superconductivity in the η -carbide-type suboxide $\text{Ti}_4\text{Ir}_2\text{O}$ with a bulk probe. Namely, the zero-temperature magnetic penetration depth $\lambda_{eff}(0)$ and the temperature as well as the field dependence of λ_{eff}^{-2} were studied by means of μSR experiments.

We have demonstrated the isotropic fully gap pairing and the preserved time-reversal symmetry in the SC state of this material. Interestingly, the T_c/λ_{eff}^{-2} ratio is comparable to those of high-temperature unconventional superconductors, pointing to the unconventional nature of superconductivity in $\text{Ti}_4\text{Ir}_2\text{O}$. This result – together with earlier findings of the high upper critical field larger than the Pauli limit and the thermodynamic signatures for an FFLO state – hints towards an unconventional pairing mechanism in this material. These results identify $\text{Ti}_4\text{Ir}_2\text{O}$ as time-reversal-invariant fully gapped unconventional superconductor.

ACKNOWLEDGMENTS

The muon spectroscopy studies were performed at the Swiss Muon Source (S μ S) Paul Scherrer Institute, Villigen, Switzerland. This work was supported by the

Swiss National Science Foundation under Grant No. PCEFP2_194183. We acknowledge Dr. Christopher Baines for the technical support provided during the experiment. Z.G. acknowledges support from the Swiss National Science Foundation (SNSF) through SNSF Start-

ing Grant (No. TMSGI2_211750). A portion of this work was performed at the National High Magnetic Field Laboratory, which is supported by National Science Foundation Cooperative Agreement No. DMR-1644779 and the State of Florida.”

-
- [1] X. Zhou, W-S Lee, M. Imada, N. Trivedi, P. Phillips, H-Y Kee, P. Törmä and M. Eremets, *Nat Rev Phys* **3**, 462–465 (2021).
- [2] J. Falson, J., Y. Xu, M. Liao, Y. Zang, K. Zhu, C. Wang, Z. Zhang, H. Liu, W. Duan, K. He, H. Liu, J.H. Smet, D. Zhang, and Q.-K. Xue, *Science* **367**, 1454 (2020).
- [3] S. Khim, J. F. Landaeta, J. Banda, N. Bannor, M. Brando, P. M. R. Brydon, D. Hafner, R. KÜchler, R. Cardoso-Gil, U. Stockert, A. P. Mackenzie, D. F. Agterberg, C. Geibel, and E. Hassinger, *Science* **373**, 1012 (2021).
- [4] F.O. von Rohr, *Chem. Mater.* **35**, 9455 (2023).
- [5] P. Fulde, *R.A. Ferrell Phys. Rev.* **135**, A550 (1964),
- [6] A.I. Larkin, Y.N. Ovchinnikov, Nonuniform state of superconductors *Sov. Phys. JETP* **20**, 762 (1965).
- [7] A.K. Clogston *Phys. Rev. Lett.* **9**, 266 (1962).
- [8] Y. Zhang, B. Wang, Z. Xiao, Y. Lu, T. Kamiya, Y. Uwatoko, H. Kageyama and H. Hosono, *npj Quantum Materials* **2**, 45 (2017).
- [9] M.D. Balestra, O. Atanov, R. Lefèvre, O. Blacque, Y.H. Ng, R. Lortz, and F.O. von Rohr, *Journal of Materials Chemistry C* **10**, 11703 (2022).
- [10] K. Ma, R. Lefevre, K. Gornicka, H. O. Jeschke, X. Zhang, Z. Guguchia, T. Klimczuk, and F O. von Rohr, *Chem. Mater.* **33**, 8722 (2021).
- [11] K. Ma, J. Lago, F. O.von Rohr, *J. Alloys Compd.* **796**, 287 (2019).
- [12] H.C. Ku and D.C. Johnston, *Chin. J. Phys.* **22**, 59 (1984).
- [13] T. Waki, S. Terazawa, T. Yamazaki, Y. Tabata, K. Sato, A. Kondo, K. Kindo, M. Yokoyama, Y. Takahashi and H. Nakamura, *Europhys. Lett.* **94**, 37004 (2011).
- [14] K. Ma, K. Gornicka, R. Lefevre, Y. Yang, H. M. Ronnow, H.O. Jeschke, T. Klimczuk, and F O. von Rohr, *ACS Mater. Au* , **1**, 55 (2021).
- [15] R. Mackay, G. J.Miller, H. F.Franzen, *J. Alloys Compd.* **204**, 109 (1994).
- [16] Bin-Bin Ruan, Meng-Hu Zhou, Qing-Song Yang, Ya-Dong Gu, Ming-Wei Ma, Gen-Fu Chen, Zhi-An Ren, *Chin. Phys. Lett.* **39**, 027401 (2022).
- [17] M. Tinkham, *Introduction to Superconductivity*. Krieger Publishing Company, Malabar, Florida, 1975.
- [18] M. L. Kiesel, C. Platt, and R. Thomale, *Phys. Rev. Lett.* **110**, 126405 (2013).
- [19] B. R. Ortiz, S. M.L. Teicher, Y. Hu, J. L. Zuo, P. M. Sarte, E. C. Schueller, A.M. Milinda Abeykoon, M. J. Krogstad, S. Rosenkranz, R. Osborn, R. Seshadri, L. Balents, J. He, and S. D. Wilson, *Phys. Rev. Lett.* **125**, 247002 (2020).
- [20] C. Mielke III, D. Das, J.-X. Yin, H. Liu, R. Gupta, Y.-X. Jiang, M. Medarde, X. Wu, H. C. Lei, J. Chang, Pengcheng Dai, Q. Si, H. Miao, R. Thomale, T. Neupert, Y. Shi, R. Khasanov, M. Z. Hasan, H. Luetkens and Z. Guguchia. Time-reversal symmetry-breaking charge order in a kagome superconductor. *Nature* **602**, 245-250 (2022).
- [21] Z. Guguchia, R. Khasanov, and H. Luetkens. Unconventional charge order and superconductivity in kagome-lattice systems as seen by muon-spin rotation. *npj Quantum Materials* **8**, 41 (2023).
- [22] J. Hu, Y.H. Ng1, O. Atanov1, B.-B. Ruan, Z.-A. Ren, and R. Lortz, preprint arXiv:2312.01914 (2023).
- [23] J. E. Sonier, J. H. Brewer, and R. F. Kiefl, *Rev. Mod. Phys.* **72**, 769 (2000).
- [24] S. Blundell, R. De Renzi, T. Lancaster, and F. Pratt, *Introduction to Muon Spectroscopy* (Oxford Univ. Press, 2021).
- [25] A. D. Hillier, S. Blundell, I. McKenzie, I. Umegaki, L. Shu, J. A. Wright, T. Prokscha, F. Bert, K. Shimomura, A. Berlie, H. Alberto and I. Watanabe, *Nat Rev Methods Primers* **2**, 4 (2022).
- [26] Z. Guguchia et al., Tunable unconventional kagome superconductivity in charge ordered RbV_3Sb_5 and KV_3Sb_5 . *Nature Communications* **14**, 153 (2023).
- [27] G. M. Luke, Y. Fudamoto, K. M. Kojima, M. I. Larkin, J. Merrin, B. Nachumi, Y. J. Uemura, Y. Maeno, Z. Q. Mao, Y. Mori, H. Nakamura and M. Sigrist. *Nature* **394**, 559 (1998).
- [28] A. D. Hillier, J. Quintanilla, and R. Cywinski, *Phys. Rev. Lett.* **105**, 229901 (2010).
- [29] J.A.T. Barker, D. Singh, A. Thamizhavel, A.D. Hillier, M.R. Lees, G. Balakrishnan, D. McK. Paul, and R.P. Singh, *Phys. Rev. Lett.* **115**, 267001 (2015)
- [30] R. P. Singh, A.D. Hillier, B. Mazidian, J. Quintanilla, J.F. Annett, D. McK. Paul, G. Balakrishnan, and M.R. Lees, *Phys. Rev. Lett.* **112**, 107002 (2014).
- [31] T. Shang, M. Smidman, S.K. Ghosh, C. Baines, L.J. Chang, D.J. Gawryluk, J.A.T. Barker, R.P. Singh, D.McK. Paul, G. Balakrishnan, E. Pomjakushina, M. Shi, M. Medarde, A.D. Hillier, H.Q. Yuan, J. Quintanilla, J. Mesot, and T. Shiroka. *Phys. Rev. Lett.* **121**, 257002 (2018)
- [32] P. K. Biswas, H. Luetkens, T. Neupert, T. Stürzer, C. Baines, G. Pascua, A. P. Schnyder, M. H. Fischer, J. Goryo, M. R. Lees, H. Maeter, F. Brückner, H.-H. Klauss, M. Nicklas, P. J. Baker, A. D. Hillier, M. Sigrist, A. Amato, and D. Johrendt. *Phys. Rev. B* **87**, 180503(R) (2013)
- [33] A. Amato, H. Luetkens, K. Sedlak, A. Stoykov, R. Scheuermann, M. Elender, A. Raselli, and D. Graf. *Review of Scientific Instruments* **88**, 093301 (2017).
- [34] A. Suter and B. Wojek, *Phys. Procedia* **30**, 69 (2012).
- [35] E. H. Brandt, *Phys. Rev. B* **37**, 2349 (1988).
- [36] E. H. Brandt, *Phys. Rev. B* **68**, 054506 (2003).
- [37] R. Prozorov and R. W. Giannetta, *Supercond. Sci. Technol.* **19**, R41 (2006).
- [38] A. Carrington and F. Manzano, *Physica C* **385**, 205 (2003).
- [39] Uemura, Y.J. et. al., Basic Similarities among Cuprate,

- Bismuthate, Organic, Chevrel Phase, and Heavy-Fermion Superconductors Shown by Penetration Depth Measurements. *Phys. Rev. Lett.* **66**, 2665 (1991).
- [40] Z. Guguchia, F. von Rohr, Z. Shermadini, A. T. Lee, S. Banerjee, A. R. Wieteska, C. A. Marianetti, B. A. Frandsen, H. Luetkens, Z. Gong, S. C. Cheung, C. Baines, A. Shengelaya, G. Taniashvili, A. N. Pasupathy, E. Morenzoni, S. J. L. Billinge, A. Amato, R. J. Cava, R. Khasanov, Y. J. Uemura, Signatures of the topological s^{+-} superconducting order parameter in the type-II Weyl semimetal T_d -MoTe₂. *Nature Communications* **8**, 1082 (2017).
- [41] von Rohr, F. O. et al. Unconventional Scaling of the Superfluid Density with the Critical Temperature in Transition Metal Dichalcogenides. *Science Advances* **5**(11), eaav8465 (2019).
- [42] D. Das et. al., Time-reversal invariant and fully gapped unconventional superconducting state in the bulk of the topological Nb_{0.25}Bi₂Se₃. *Phys. Rev. B* **102**, 134514 (2020).
- [43] J. Hu et. al., Thermodynamic evidence for the Fulde-Ferrell-Larkin Ovchinnikov state in the isotropic superconductor Ti₄Ir₂O. arXiv:2312.01914 (2023).